# An Intravascular Ultrasound-based Tissue Characterization Using Shift-invariant Features Extracted by Adaptive Subspace SOM

Ryosuke Kubota, Mami Kunihiro, Noriaki Suetake, Eiji Uchino,
Genta Hashimoto, Takafumi Hiro, and Masunori Matsuzaki

***Abstract*—Tissue characterization of a plaque is important for a diagnosis of the acute coronary syndromes (ACS). An intravascular ultrasound (IVUS) technique with a probe mounted at the tip of a catheter is often used. As the conventional tissue characterization methods using the IVUS technique, an integrated backscatter (IB) analysis in the time domain and a spectral analysis in the frequency domain have been proposed so far. However, those conventional methods can not perform a good classification. The IB values are substantially affected by the intensity of the backscattered ultrasound, and the frequency characteristics of some types of tissues are similar with others.**

**In this paper, we propose a novel tissue characterization method by using an adaptive subspace self-organizing map (ASSOM). ASSOM can extract various features from the IVUS signal. Those features are suitable for the tissue characterization, because the overlap of the distributions of the extracted features is much smaller than the one, e.g., by the IB analysis or by a traditional Fourier spectrum analysis. A tissue is characterized by using the statistical information of the features extracted by ASSOM. Through the application to the tissue characterization of the real IVUS signal, the performance of the proposed method has been verified by comparing it with the conventional methods.**

***Keywords*—Self-organizing map (SOM), adaptive subspace self-organizing map (ASSOM), discriminant analysis, acute coronary syndrome (ACS), intravascular ultrasound (IVUS), tissue characterization.**

## I. Introduction

Rupture of vulnerable atherosclerotic plaque is a cause of most acute coronary syndromes (ACS) [1], [2]. It has been reported that the risk of plaque rupture depends on plaque type (composition), i.e., stabilities of the atherosclerotic plaques are considerably related to their histological compositions [3]. It is thus important to investigate their compositions in order for an early stage detection of the vulnerable atheroma before rupture. That is, the precise characterization of the tissues of atherosclerotic plaque is strongly required in clinical practice.

Manuscript received December 31, 2008; revised December 31, 2008.

R. Kubota is with the Departmentof Intelligent Systems Engineering, Ube National College of Technology, 2-14-1 Tokiwadai, Ube 755-8555, Japan, e-mail: kubota@ube-k.ac.jp.

M. Kunihiro, N. Suetake and E. Uchino are with the Graduate School of Sciencee and Engineering, Yamaguchi University, 1677-1 Yoshida, Yamaguchi 753-8512, Japan, e-mail: {kunihiro, suetake, uchino}@ic.sci.yamaguchi-u.ac.jp.

G. Hashimoto, T. Hiro and M. Matsuzaki are with the Graduate School of Medicine, Yamaguchi University, 1-1-1 Minami-kogushi, Ube 755-8555, Japan.

A backscattered intravascular ultrasound (IVUS) method, which is one of the popular imaging techniques, provides tomographic visualization of coronary artery [4], [5]. The IVUS method gives a real-time imaging of the plaque in vivo, and has been employed for an analysis of ACS [6]-[11].

As the conventional tissue characterization methods with the IVUS technique, an integrated backscatter (IB) analysis in the time domain has been proposed so far [12], [13]. In this analysis, a tissue is classified by an IB value, which is a locally averaged power of a backscattered ultrasound. The IB analysis is effective in a restricted case. It is not however always useful for the characterization of the tissues, because IB values are substantially affected by the intensity of the backscattered ultrasound. The intensity of the ultrasound depends on the distance between the plaque and the probe. It is thus not easy to classify the tissues of the plaque only by the IB values.

The spectral analysis of the backscattered IVUS radiofrequency (RF) signal in the frequency domain seems to be one approach for this problem [5], [14], [15]. In this analysis, the pixel in the IVUS image is classified by the feature vector, which is a Fourier spectrum of the local RF signal. However the frequency characteristics of some tissues are also similar.

On the other hand, a k-nearest neighbor (kNN) method [16] is a currently well-known classification method to classify the unknown input feature vector by the training vectors. The kNN is the most popular method for the supervised statistical classification problems, and is applied to various pattern recognition and classification problems [17], [18]. It is an extension of a nearest neighbor classification [19]-[22], which is one of the popular nonparametric classification methods. The kNN is a flexible and robust classification method without any preprocessing of the training feature vectors. However, the kNN can not perform a satisfactory classification in case where the distribution of the feature vectors overlaps with each other.

In this paper, we propose a novel tissue characterization method by using an adaptive subspace self-organizing map (ASSOM) [23]. ASSOM has a modular neural network architecture, the modules of which learn to identify input patterns subject to some simple transformations, e.g., shifted, rotated, or scaled. The learning process is unsupervised and competitive which is related to that of the traditional self-organizing map (SOM) [24], [25]. ASSOM has been applied to various pattern recognition and feature extraction problems so far [26]-[30].

The proposed method involves two stages, which are a

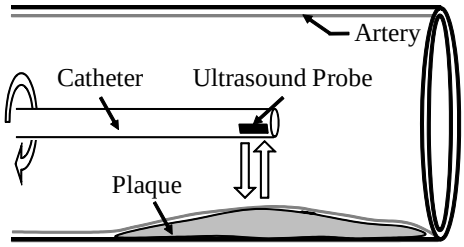


Fig. 1. An ultrasound probe mounted at the tip of a catheter.

feature extraction stage by ASSOM and a classification stage for an ultrasound RF signal reflected from the tissue of plaque. In the feature extraction stage, ASSOM produces various linear subspaces for feature extraction from an ultrasound RF signal reflected from the tissues. The feature vectors are then extracted by ASSOM. The classification stage is followed by the feature extraction stage. The present method uses the statistical information of the extracted feature vectors, which is a similarity measure among the distributions of feature vectors obtained from the tissues. A Mahalanobis' generalized distance (MGD) is employed for this measure.

The validity and the effectiveness of the proposed method are verified by applying it to the tissue characterization problem of the real IVUS signal.

## II. Conventional Tissue Characterization Using Intravascular Ultrasound Method

### A. Intravascular Ultrasound (IVUS) Method

An IVUS method is very useful because it facilitates a real-time imaging in vivo, and provides a 2-dimensional cross sectional image called an IVUS "B-mode" image [5].

The IVUS image is made-up of a radiofrequency (RF) signal reflected from the tissue. In the IVUS method, the ultrasound probe mounted at the tip of the catheter is inserted in the coronary artery as shown in Fig.1. The ultrasound signal is transmitted from the probe, and the backscattered RF signal from the tissue is also received by its probe. The probe rotates in the arterial lumen iterating those operations. The transmitting frequency of ultrasound is 40 MHz, and the backscattered RF signal is sampled at 400 MHz.

The sampled RF signal shown in Fig.2 (a) is first transformed into an 8-bit intensity signal shown in Fig.2 (b) by taking the absolute-, the envelope-, and the logarithm-operations for the RF signal. The intensity signals in all radial directions are then used to construct a tomographic cross sectional image of a coronary artery as shown in Fig.2 (c). The IVUS image of Fig.2 (c) is constructed with 2,048 pixels in depth from the center, and 256 lines in radial direction.

### B. Conventional Tissue Characterization Methods

As one of the IVUS-based conventional tissue characterization methods, an integrated backscatter (IB) analysis is a popular one [12], [13]. In this analysis, a tissue is classified by using a one-dimensional feature, i.e., IB value, which is a locally averaged power of a backscattered RF signal. Here let

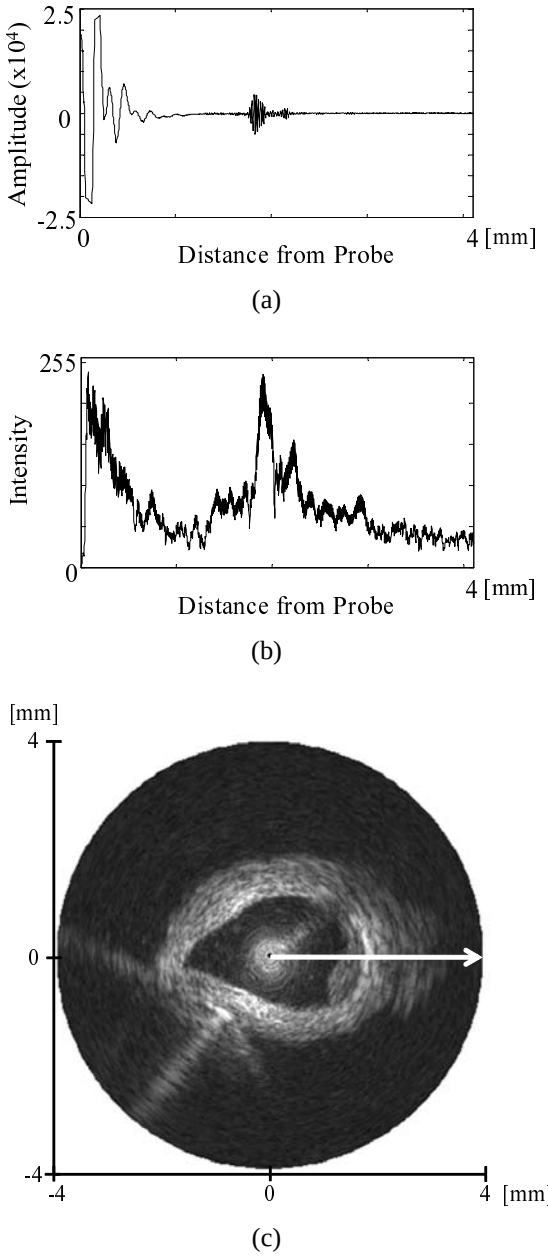


Fig. 2. Examples of an RF signal and a B-mode image obtained by the IVUS method. (a) Received RF signal; (b) Intensity signal of (a); (c) B-mode image. Vertical axes of (a) and (b) correspond to the arrowed line in the image (c). In each vertical axis, 4 [mm] corresponds to 2,048 pixels.

$x(t)$ and $x_0(t)$ be an amplitude of the sampled backscattered RF signal and the smallest signal which can be sensed by the probe at point $t$, respectively. IB value at point $t$ is given by:

$$IBS(t) = 20\log\left(\frac{\frac{1}{T+1}\sum_{i=t-T/2}^{t+T/2} x(i)^2}{\frac{1}{T+1}\sum_{i=t-T/2}^{t+T/2} x_0(i)^2}\right), \qquad (1)$$

where $T$ is a constant to decide a window size for the calculation of IB value.

The IB analysis is not always accurate to classify the tissues

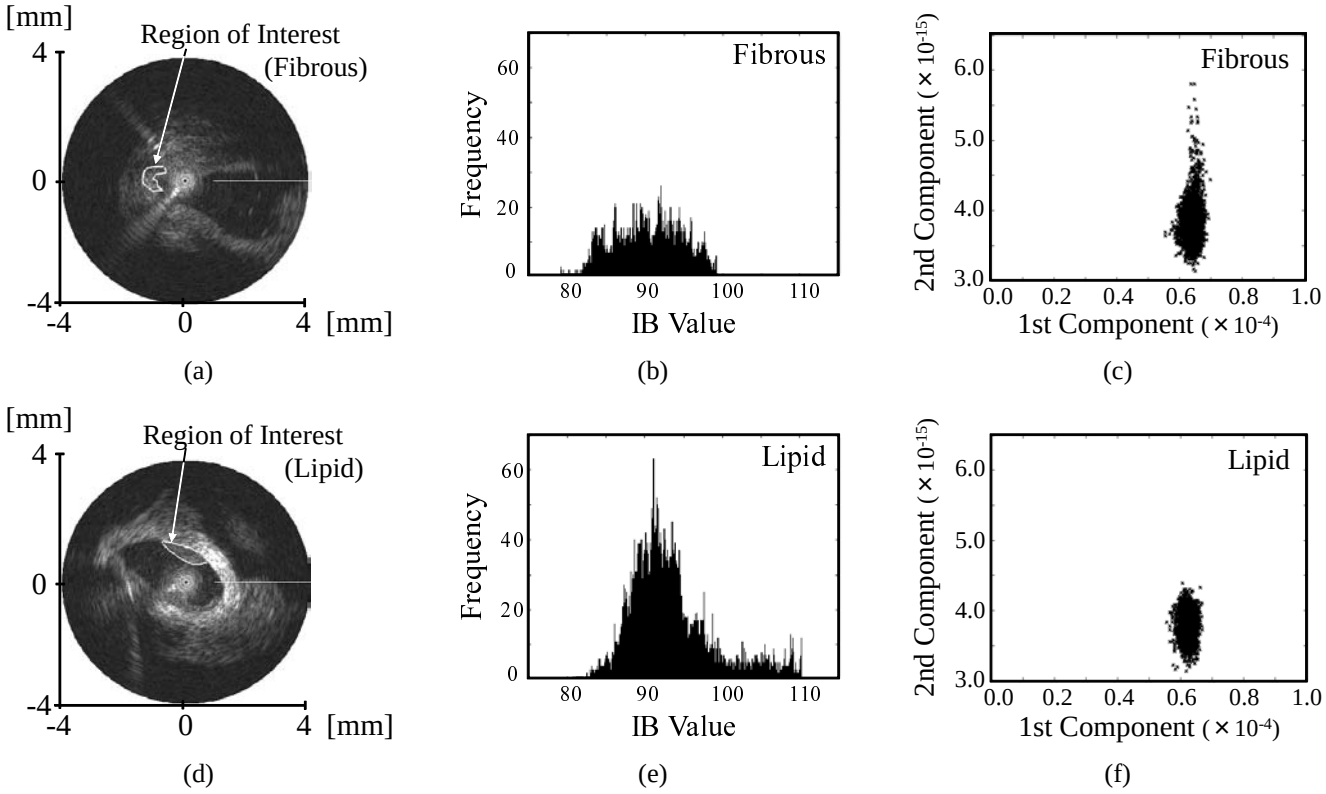


Fig. 3. Distributions of the feature vectors employed in the conventional methods for tissue characterization. (a) An example of fibrous plaque; (b) Distribution of the IB values for fibrous plaque of (a); (c) Distribution of the Fourier power spectra for fibrous plaque of (a) in 2D; (b) An example of lipid plaque; (e) Distribution of the IB values for lipid plaque of (d); (f) Distribution of the Fourier power spectra for lipid plaque of (b) in 2D.

of plaque, because some types of tissues have similar IB values with others. Further, it is not easy to classify the tissues only by the IB value, because it is the locally averaged power of RF signal and the power of RF signal is substantially affected by the distance between the plaque and the probe. That is, if the probe is near the plaque, the IB value becomes big, and if the probe is far from the plaque, the IB value becomes small. The position of the probe in the coronary artery can not be controlled.

On the other hand, a spectral analysis in the frequency domain has been proposed so far [5]-[15]. In the spectral analysis, the tissue is classified by the logarithmic Fourier power spectrum of the local RF signal. The Fourier power spectrum is calculated by the short-time fast Fourier transform (FFT) of the RF signal $x(t)$ in depth direction. The conventional tissue characterization methods based on the spectrum analysis use the components of various frequency bands. However, the frequency characteristics of some tissues are also similar here.

Figs.3 (b) and (e) show the distributions of the IB values for fibrous and lipid plaques of Fig.3 (a) and (d), respectively. Figs.3 (c) and (f) show the distributions of the Fourier power spectra for the plaques of Fig.3 (a) and (d) compressed in 2D by a multiple discriminant analysis (MDA) [16]. MDA is one of the data compression method which maximizes the difference of data in each class. The details of MDA are described in Chapter 3.

It is seen from Fig.3 that the distributions of the feature vectors widely overlap with each other. A precise tissue characterization by using the traditional pattern classification methods with those feature vectors is thus difficult.

## III. Proposed Tissue Characterization Method by Adaptive Subspace Self-Organizing Map

The method proposed in this paper consists of two stages. Those are a feature extraction stage by using an adaptive subspace self-organizing map (ASSOM) and a classification stage by considering a statistical information on distributions of the extracted feature vectors.

### *A. Feature Extraction Stage by ASSOM*

In this stage, features of backscattered RF signal are extracted by ASSOM. An ordinary self-organizing map (SOM) [25] has been used in various feature extraction and pattern classification problems so far [27], [28]. However, in the ordinary SOM, the transformed patterns, such as shifted, rotated, or scaled patterns, cannot be recognized to be the same pattern. ASSOM was proposed to deal with this problem [23].

Fig.4 shows a structure of an ordinary SOM. SOM has an input layer and a competitive layer. Those layers are constructed by some units. In the ordinary SOM, each unit on the competitive layer is characterized by one weight vector. A similarity between the input vector and the weight vector assigned to each unit is evaluated based on the Euclidean distance or the inner product between them.

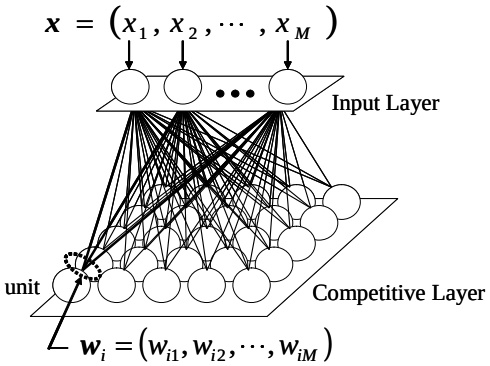


Fig. 4. A structure of an ordinary SOM.

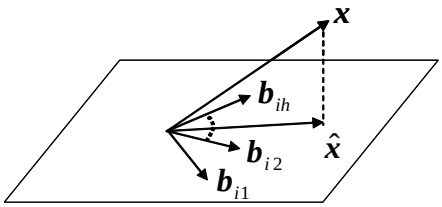


Fig. 5. A projection $\hat{\boldsymbol{x}}$ of an input vector $\boldsymbol{x}$ onto the linear subspace of the module of ASSOM.

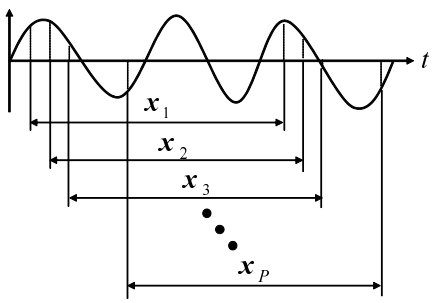


Fig. 6. An example of an episode.

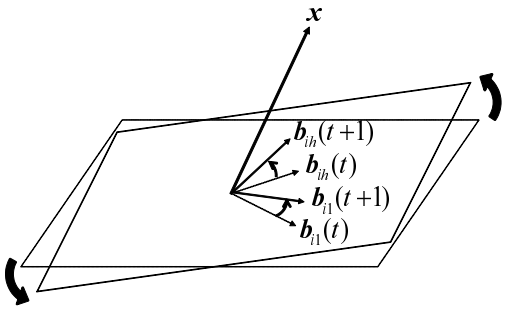


Fig. 7. An update of the linear subspace of the $i$-th module of ASSOM.

In ASSOM on the other hand, the $i$-th module (corresponding to a unit on the competitive layer in the ordinary SOM) is characterized by a linear subspace which consists of $h$ basis vectors $\boldsymbol{b}_{im}(m = 1, 2, \cdots, h)$. In order to evaluate the degree to which the input vector lies on the linear subspace of the module (unit) of ASSOM, the input vector $\boldsymbol{x}$ is projected onto the linear subspace as shown in Fig.5. The degree is evaluated by a norm $\|\hat{\boldsymbol{x}}\|$ (a projection of $\boldsymbol{x}$ onto the linear subspace of ASSOM module).

ASSOM employs an "episode" input. Consider the sinusoidal wave shown in Fig.6. Let $\boldsymbol{x}_j$ be a section of the sinusoidal wave, and let $s = \{\boldsymbol{x}_j; j = 1, 2, \cdots, P\}$ be a set of temporal subsequent sequences, i.e., the episode. The best matching module (the representative winner module), which has the maximum value of $\|\hat{\boldsymbol{x}}_{ij}\|$, is decided by:

$$z = \arg\max_i \sum_{j \in s} \|\hat{\boldsymbol{x}}_{ij}\|, \tag{2}$$

where $\hat{\boldsymbol{x}}_{ij}$ is a projection of the $j$-th input vector $\boldsymbol{x}_j$ in the episode onto the linear subspace spanned by the basis vectors $\boldsymbol{b}_{im}$ in the $i$-th module of ASSOM. $\hat{\boldsymbol{x}}_{ij}$ is calculated by:

$$\hat{\boldsymbol{x}}_{ij} = \sum_{m=1}^{h} \left( \boldsymbol{b}_{im}^T \cdot \boldsymbol{x}_{ij} \right) \boldsymbol{b}_{im}, \tag{3}$$

where "$\cdot$" means scalar product and $T$ is a transpose operation.

The basis vectors in each module are updated as follows so as to rotate each linear subspace towards the input vector (see Fig.7):

$$\boldsymbol{b}_{im}(t+1) = \prod_{j \in s} \left[ \boldsymbol{I} + \alpha(t) H(t) \frac{\boldsymbol{x}_j \cdot \boldsymbol{x}_j^T}{\|\hat{\boldsymbol{x}_{ji}}\| \|\boldsymbol{x}_j\|} \right] \boldsymbol{b}_{im}(t), \tag{4}$$

where $H(t)$ is an ordinary gaussian-type neigborhood function given by:

$$H(t) = \exp\left( -\frac{\|\boldsymbol{p}_z - \boldsymbol{p}_i\|^2}{h(t)^2} \right), \tag{5}$$

where $\boldsymbol{p}_z$ and $\boldsymbol{p}_i$ are the positions of the representative winner module and the $i$-th module on the competitive layer, respectively. $\alpha(t)$ and $h(t)$ are a learning ratio and a neighboring coefficient which monotonously decrease as the learning proceeds. $\boldsymbol{I}$ is a unit matrix.

Because of the learning characteristics of ASSOM using subspace and episode, the transformed patterns, e.g., shifted, rotated, or scaled patterns, can then be identified and classified properly to be the same patterns. Furthermore the input vectors with similar features are allocated in the neighboring modules. The linear subspace of ASSOM thus becomes spatially ordered on the competitive layer.

In the feature extraction stage, various patterns of backscattered RF signals of the fibrous and the lipid tissues are first grasped by learning on the linear subspaces (modules) of ASSOM.

The feature vectors $\boldsymbol{v} = (v_1, v_2, \cdots, v_M)^T$ for classification of the fibrous and the lipid tissues are calculated by:

$$v_i = \sum_{j \in s} \|\hat{\boldsymbol{x}}_{ij}\|, (i = 1, 2, \cdots, M). \tag{6}$$

$v_i$ is a degree of response to the episode, from the linear subspace of the $i$-th module of ASSOM. The feature vector thus means a set of similarities for various patterns of input.

*B. Classification Stage Using Feature Vectors Extracted by ASSOM*

The $M$-dimensional feature vectors extracted by ASSOM are first compressed into the 2-dimensional space by a multiple

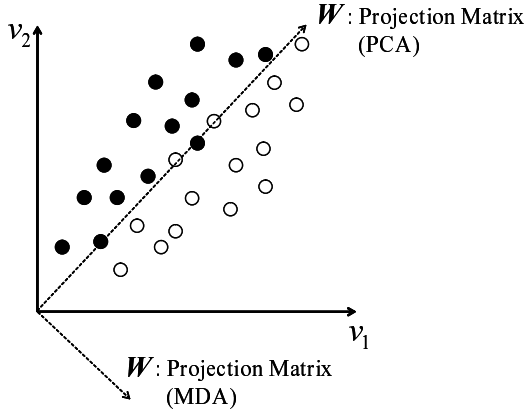


Fig. 8. An example of a multiple discriminant analysis of 2D data with 2-class. ○: Data belonging to class 1; ●: Data belonging to class 2;

discriminant analysis (MDA) [16]. MDA is similar to a principal component analysis (PCA). MDA and PCA are however mathematically different in what they maximize. Fig.8 shows an example of projection by MDA or PCA. PCA maximizes the variance of all data. MDA, on the contrary, maximizes a degree of separation of data in each class.

In the 2-class MDA, let $\boldsymbol{S}_B$ be a between-class scatter matrix defined by:

$$\boldsymbol{S}_B = \sum_{\ell=1}^{2} N_\ell (\boldsymbol{\mu}_\ell - \boldsymbol{\mu})(\boldsymbol{\mu}_\ell - \boldsymbol{\mu})^T, \tag{7}$$

and $\boldsymbol{S}_W$ be a within-class scatter matrix defined by:

$$\boldsymbol{S}_W = \sum_{\ell=1}^{2} \sum_{\boldsymbol{v} \in \chi_\ell} (\boldsymbol{v} - \boldsymbol{\mu}_\ell)(\boldsymbol{v} - \boldsymbol{\mu}_\ell)^T, \tag{8}$$

where $N_\ell$, $\boldsymbol{\mu}_\ell$ and $\chi_\ell$ are a number of the feature vectors, an average and a set of the feature vectors in the $\ell$-th class. $\boldsymbol{\mu}$ stands for an average of all the feature vectors in both classes.

The evaluation function $J(\boldsymbol{W})$, which is a degree of separation of data in each class, is defined by:

$$J(\boldsymbol{W}) = \frac{|\boldsymbol{W}^T \boldsymbol{S}_B \boldsymbol{W}|}{|\boldsymbol{W}^T \boldsymbol{S}_W \boldsymbol{W}|}, \tag{9}$$

where $\boldsymbol{W}$ is a projection matrix from a high dimensional space onto a low dimensional space. $\boldsymbol{W}$ is calculated so as to maximize $J(\boldsymbol{W})$. The compressed feature vector $\boldsymbol{v}' = \boldsymbol{W}^* \boldsymbol{v}$ is used for classification, where $\boldsymbol{W}^*$ is an optimum projection matrix.

Fig.9 shows a conceptual sketch of the proposed classification method. The proposed method uses the distribution of the compressed feature vectors. Let $\chi_\ell$ $(\ell = 1, 2, \cdots, L)$ be a set of the training feature vectors in the $\ell$-th class. In case of Fig.9, a number of classes $L$ is 2 (fibrous and lipid classes). To classify the feature vector obtained at point $\boldsymbol{p}$ of concern on the IVUS image space, the proposed method considers a set of the new feature vectors obtained at the neighboring points around $\boldsymbol{p}$ as shown in Fig.9. Let $\chi$ be a set of the feature vectors, which are compressed by $\boldsymbol{W}^*$, obtained at the points $\{\boldsymbol{p}_k; k = 1, 2, \cdots, K\}$.

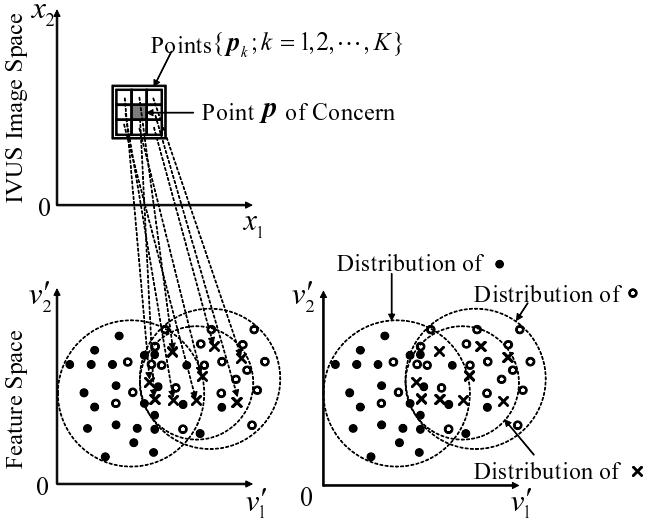


Fig. 9. A conceptual sketch of the proposed classification method. ○: Training feature vectors belonging to class 1; ●: Training feature vectors belonging to class 2; ×: Feature vectors obtained at points $\boldsymbol{p}_k$ on the IVUS image space.

In the proposed method, a similarity between the distribution of the $K$ feature vectors in $\chi$ and that of the training feature vectors in $\chi_\ell$ is calculated by using a Mahalanobis' generalized distance (MGD) as follows:

$$D(\chi, \chi_\ell) = (\boldsymbol{m}' - \boldsymbol{\mu}'_\ell)^T \Sigma_W^{-1} (\boldsymbol{m}' - \boldsymbol{\mu}'_\ell), \tag{10}$$

where $\boldsymbol{m}'$ and $\boldsymbol{\mu}'_\ell$ are an average of the compressed feature vectors belonging to $\chi$ or $\chi_\ell$, respectively. $\Sigma_W$ is a within-class scatter matrix calculated by:

$$\begin{aligned} \Sigma_W &= \frac{1}{K} \sum_{\boldsymbol{v}' \in \chi} (\boldsymbol{v}' - \boldsymbol{\mu}')(\boldsymbol{v}' - \boldsymbol{\mu}')^T \\ &+ \frac{1}{N_\ell} \sum_{\boldsymbol{v}' \in \chi_\ell} (\boldsymbol{v}' - \boldsymbol{\mu}'_\ell)(\boldsymbol{v}' - \boldsymbol{\mu}'_\ell)^T. \end{aligned} \tag{11}$$

The feature vector obtained at point $\boldsymbol{p}$ of concern is thus classified into the class $c$ as follows:

$$c = \arg\min_{\ell} D(\chi, \chi_\ell). \tag{12}$$

## IV. Simulation and Experimental Results

In order to verify the validity and the practical effectiveness of the proposed method (feature extraction by ASSOM and MGD-based classification), it is first applied to the toy classification problem, and then to the coronary tissue characterization problem of the real IVUS data [12]-[15].

### A. Classification Results of Toy Problem

As a general application example of the proposed MGD-based classification method, we first apply it to the ordinary 3-dimensional 3-class pixel classification problem.

The precise pixel classification is very important for a land-cover classification problem [31]. In this problem, a land coverage is classified by remote sensing images, e.g., the LANDSAT images and the synthetic apeture radar (SAR) images. However, it is difficult to obtain the precise feature

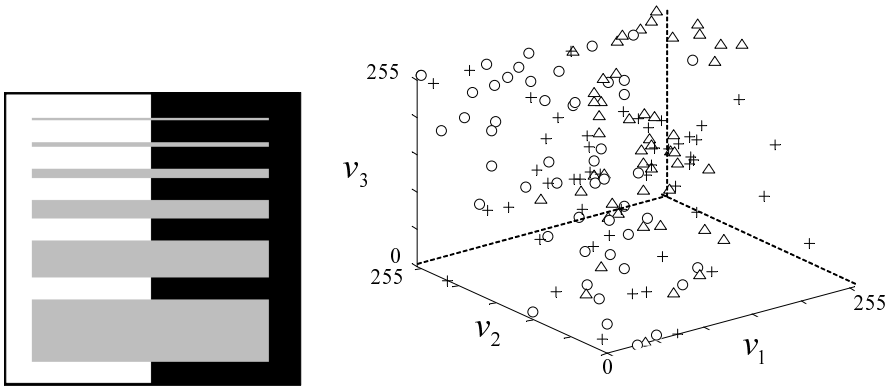


(a) (b)

Fig. 10. A toy classification problem of 3-class with 3-dimensional feature vectors. (a) Original noiseless image; (b) Distribution of the obtained feature vectors (RGB components); $\triangle$, $\bigcirc$ and $+$ are the data obtained from the white (red), gray (green) and black (blue) area, respectively.

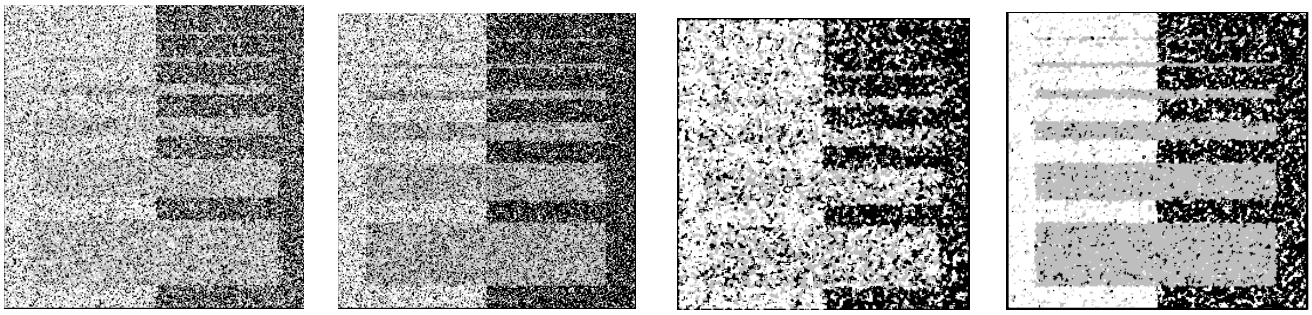

(a) (b) (c) (d)

Fig. 11. Classification results for Fig.10 (a). (a) kNN ($k=1$); (b) kNN ($k=9$); (c) Mode filter ($3\times3$) with kNN ($k=1$); (d) Proposed method ($3\times3$).

vectors from the observation data, because the actually observed data contain various noises and measuring errors.

The data assigned to each pixel in the image are the observation data acquired by the sensors with different frequency bands. Data observed at each pixel are classified into 3 classes shown in Fig.10 (a) ($256 \times 256$ pixels). The component data of each pixel are shown in Fig.10 (b). In the ordinary color remote sensing images, they are RGB components of the image. Red, green, and blue are replaced with white, gray, black in this experiment, respectively, for black and white printing sake. The resolution is 8 bit/pixel for each RGB component which is scaled in full contrast. In this test problem, the RGB components are to be the same when observed from the pixel in the same area. However, in general, they are disturbed by noise and then distributed as shown in Fig.10 (b).

The proposed classification method is applied to this test classification problem. The reason why the geometric pattern of Fig.10 (a) is employed is to evaluate the fineness of classification of the proposed method. The distribution of the feature vectors of each class, i.e., the distribution of RGB components in Fig.10 (b) is given in this example by normal distribution. That is, the averages of R, G and B components for $\triangle$, $\bigcirc$ and $+$ are $(170, 85, 85)$, $(85, 170, 85)$ and $(85, 85, 170)$, respectively. Variances are 60, 80 and 100 for R, G and B components, respectively.

The classification performance of the proposed method is compared with the conventional pixel classification methods, e.g., an ordinary k-nearest neighbor (kNN) method and a mode filter [32]. The number of nearest neighbors in kNN method is ($k=1 and 9$). The mode filter employed here is with 9 pixels (3×3 window), which corresponds to the ordinary kNN ($k=1$) with mode filtering ($3\times3$). The number of the training feature vectors of each class for kNN and the proposed method is 50, i.e., the number of all training feature vectors is $150$ ($3\times50$). The training feature vectors are picked up from some areas of the observed image whose classes are known in advance. The window size of the proposed method is $3 \times 3$.

Fig.11 shows the classification results by the kNN ($k=1$, 9), the mode filter with kNN ($k = 1$), and the proposed method. It is seen that many pixels are misclassified by the conventional methods as shown in Figs.11 (a)-(c) (the desirable classification result is Fig.10 (a)). On the contrary, the proposed method gives a good classification result with fine precision as shown in Fig.11 (d). In addition, the proposed method can classify accurately even the very narrow rectangle area in the observation space. Further, it can grasp well the edge of the area.

For the quantitative evaluation of the results, we define the classification rate $E$ by:

$$E = \frac{N_{correct}}{N_{all}}, \tag{13}$$

TABLE I
AVERAGES AND STANDARD DEVIATIONS OF THE CLASSIFICATION RATE $E$ FOR EACH METHOD IN THE 3-DIMENSIONAL 3-CLASS CLASSIFICATION PROBLEM.

| Method | Average | Standard Deviation |
|---|---|---|
| kNN ($k=1$) | 0.553 | 0.195 |
| kNN ($k=9$) | 0.632 | 0.203 |
| Mode Filter ($3\times3$) | 0.769 | 0.441 |
| Proposed Method ($3\times3$) | 0.858 | 0.074 |

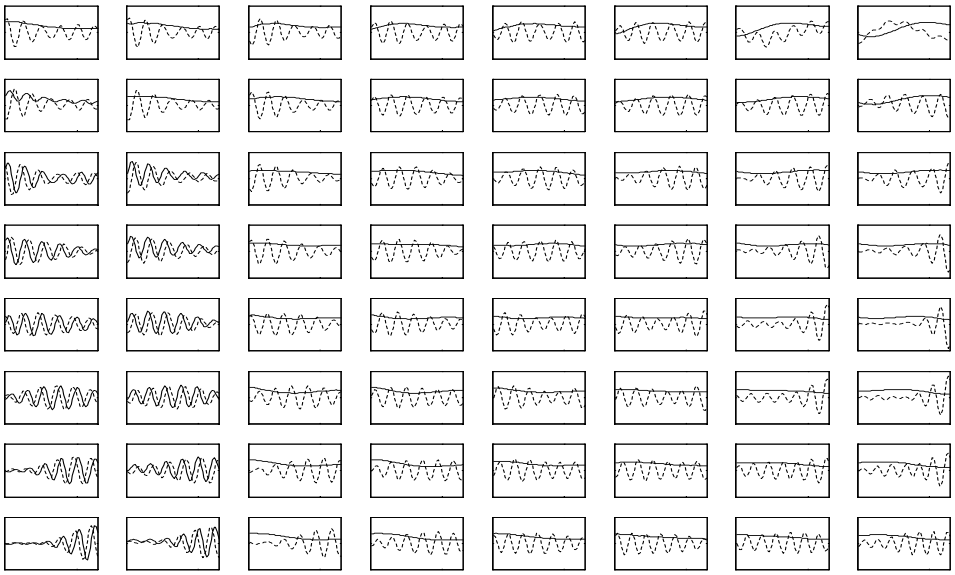

Fig. 12. Extracted basis vectors of each module of ASSOM after learning. The solid and dashed wave patterns in each graph are the basis vectors $\boldsymbol{b}_{i1}$ and $\boldsymbol{b}_{i2}$ of the $i$-th module, respectively. 2D latice of the graphs shows the positions of the modules on the competitive layer of ASSOM.

where $N_{correct}$ and $N_{all}$ represent the number of the data correctly classified and the number of all data to be classified, respectively. In order to verify statistically the effectiveness of the proposed method, the averages and the standard deviations of $E$ are calculated for 100 trials. Different feature vectors (different RGB components) are generated and then given to each pixel for each trial, although their statistical characteristics are the same for all the trials.

Table I shows the averages and the standard deviations of $E$ for the conventional and the proposed methods. It can be said that the proposed method gives the most effective and stable classification result compared with the other conventional methods.

### *B. Feature Extraction and Tissue Characterization Results Applied to Intravascular Ultrasound Signal*

The proposed method is applied to a tissue characterization problem of a real IVUS signal. The backscattered ultrasound RF signals reflected from the tissues in each region of interest (ROI) shown in Figs.3 (a) and (d), are applied as the input signals to ASSOM.

The parameters of ASSOM for the learning are: the number of modules on the competitive layer is 64 ($8\times8$); the number of vectors in the episode is 16; the number of basis vectors in a module is 2; the number of elements in each vector is 64; the initial value of the learning rate is 0.01; the initial value of the neighboring coefficient is 8; the number of learning iteration times is $2\times10^5$.

Fig.12 shows the extracted basis vectors assigned to each module of ASSOM after learning. Figs.13 (a) and (b) show the distributions of the 2-dimensional feature vectors obtained by ASSOM are which compressed by MDA. It is observed from those results that the overlap of the distributions of the feature vectors is smaller for ASSOM than for the conventional IB values or for the Fourier spectrum analysis shown in Figs.3 (b) and (e), (c) and (f).

In order to confirm the feature extraction ability of ASSOM, the overlap of the distributions is evaluated quantitatively by the sum of the contributing ratios up to the second components of MDA. The ratio of the between-class to the within-class variance of each distribution of Figs.13 (a) and (b) is also calculated. It is defined as follows:

$$J_\sigma = \frac{\sum_{k=1}^{2} n_k \left(\boldsymbol{m}'_k - \boldsymbol{m}'\right)^T \left(\boldsymbol{m}'_k - \boldsymbol{m}'\right)}{\sum_{k=1}^{2} \sum_{\boldsymbol{v}' \in \chi'_k} \left(\boldsymbol{v}' - \boldsymbol{m}'_k\right)^T \left(\boldsymbol{v}' - \boldsymbol{m}'_k\right)}, \qquad (14)$$

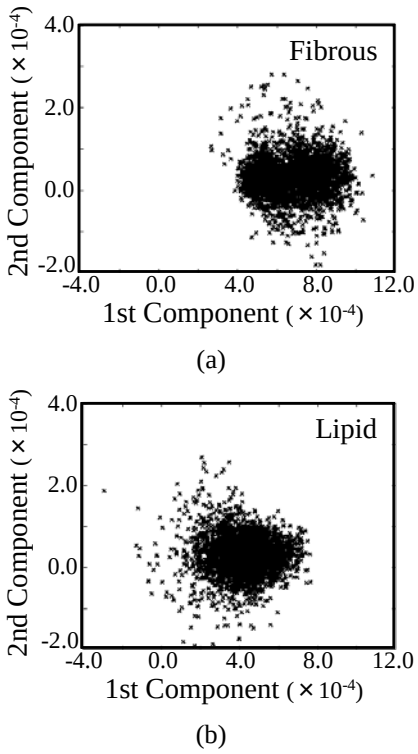


Fig. 13. Distribution of the obtained feature vectors by ASSOM. (a) Feature vectors for fibrous tissue of Fig.3 (a) compressed in 2D; (b) Feature vectors for lipid tissue of Fig.3 (b) compressed in 2D.

TABLE II
EVALUATION OF THE OVERLAP OF THE FEATURE VECTORS OF EACH METHOD.

| | Sum of the contributing ratios up to the 2nd components | $J_\sigma$ |
|---|---|---|
| Fourier Spectrum Analysis | 0.4553 | 0.4461 |
| Proposed Method | 0.6835 | 0.6177 |

where $\boldsymbol{v}'$ is a projection of $\boldsymbol{v}$ onto the 2D space by MDA. $\boldsymbol{m}'_k$ and $\chi'_k$ are an average and a set of the projected feature vectors $\boldsymbol{v}'$ in the $k$-th class, respectively. $\boldsymbol{m}'$ stands for an average of all projected feature vectors in both classes. $J_\sigma$ is positive $J_\sigma \geq 0$, and it becomes bigger according as the distributions of two classes become apart with each other.

Table II shows the sum of the contributing ratios up to the second components of MDA. The ratio of the between-class to the within-class variance is also shown. The results show that the feature vectors of the fibrous and the lipid tissues obtained by ASSOM are better spread out than those obtained by the Fourier spectrum analysis. Furthermore, the overlap of the distributions of those feature vectors is smaller for the proposed method than for the Fourier spectrum analysis.

In the classification stage, the feature vectors obtained from each ROI of Figs.3 (a) and (d) are used as the training feature vectors for classification. The classification is executed for each ROI shown in Figs.14 (a) and (c). In this classification, the tissues of plaque are classified into fibrous and lipid tissues. Figs.14 (b) and (d) are the microscope images of the stained tissue of each ROI, which are diagnosed to be fibrous and lipid tissues, respectively.

TABLE III
TISSUE CHARACTERIZATION PERFORMANCE BY EACH METHOD.

| | Fibrous | Lipid |
|---|---|---|
| IB Method | 0.27 | 0.47 |
| kNN Method | 0.55 | 0.60 |
| Fourier Spectrum Analysis Method | 0.89 | 0.18 |
| Proposed Method | 0.91 | 0.76 |

The classification performance of the proposed method using ASSOM is compared to that of the IB method, the kNN method, and the classification method based on the normal Fourier spectrum analysis. The window size of the proposed method is $3 \times 3$. The IB value, which is an averaged power of the local RF signal, is calculated at each point of a cross section of a coronary artery by shifting the window of a size of 64 points in depth direction along a radial line. The parameter of the ordinary kNN is $k = 9$.

Figs.15 and 16 show the classification results for Figs.14 (a) and (c). The white and gray areas in Figs.15 and 16 correspond to the fibrous and the lipid tissues, respectively. Many pixels are misclassified by the conventional methods. In contrast, the classification results by the proposed method are in a good coincidence with the pre-diagnosed results shown in Figs.14 (b) and (d).

For the quantitative evaluation of these results, Table III shows the correct characterization rate defined by Eq.(13). It is seen that the proposed method gives a fine characterization for both the fibrous and the lipid tissues.

With those experiments, the superiority of the proposed method over the conventional ones has been confirmed.

## V. CONCLUSION

In this paper, we have proposed a novel tissue characterization method. The present method first extracts various shift-invariant feature vectors from the RF signal by an adaptive subspace self-organizing map (ASSOM). A tissue is then classified with considering statistical similarities among the distributions of the feature vectors. The present method can performs effective feature extraction, and also characterize the tissues of plaque precisely.

Future work is an application of the present method to many types of classification problems.

## ACKNOWLEDGMENT

This work was supported in part by "Knowledge Cluster Initiative Project," for 2004-2009, funded by Japan Ministry of Education, Culture, Sports, Science and Technology.

## REFERENCES

[1] E. Falk, "Why do plaque rupture?," *Circulation*, vol.86, pp.30-42, 1992.
[2] E. Falk, P. K. Shah, V. Fuster, "Coronary plaque disruption," *Circulation*, vol.92, pp.657-671, 1995.
[3] G. J. Friedrich, N. Y. Moes, V. A. Muhlberger, C. Gabl, G. Mikuz, D. Hausmann, P. J. Fitzgerald, P. G. Yock, "Detection of intralesional calcium by intracoronary ultrasound depends on the histologic pattern," *Am Heart J.*, vol.128, pp.435-441, 1994.
[4] J. B. Hodgson, S. P. Graham, A. D. Savakus, S. G. Dame, D. N. Stephens, P. S. Dhillon, D. Brands, H. Sheehan, M. J. Eberle, "Clinical percutaneous imaging of coronary anatomy using an over-the-wire ultrasound catheter system," *Int. J. Cardiac Imaging*, vol.4, pp.187-193, 1989.

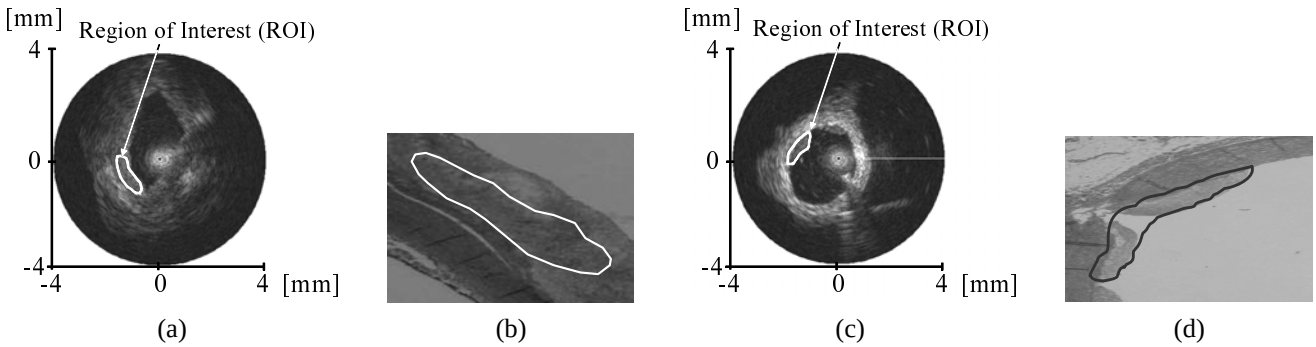


Fig. 14. Test IVUS images. (a) IVUS image with fibrous tissue; (b) Microscope image of (a); (c) IVUS image with lipid tissue; (d) Microscope image of (c).

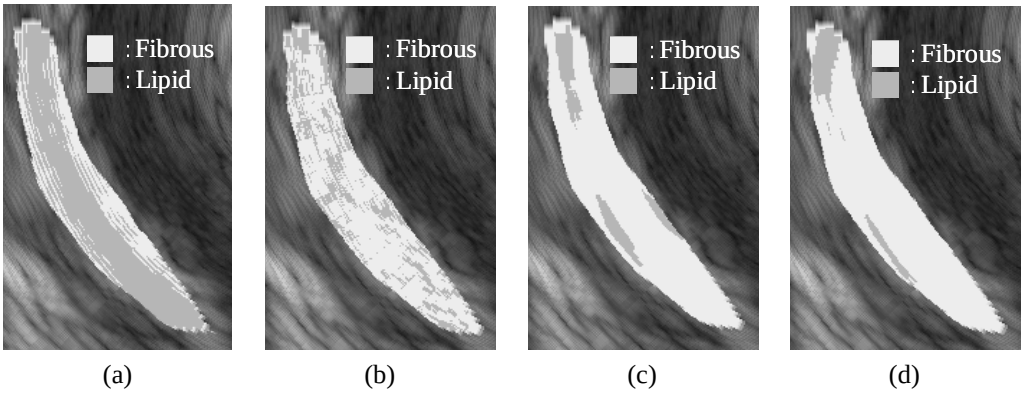


Fig. 15. Tissue characterization results for the fibrous tissue. (a) IB method; (b) kNN method; (c) Fourier spectrum analysis method; (d) Proposed method (ASSOM).

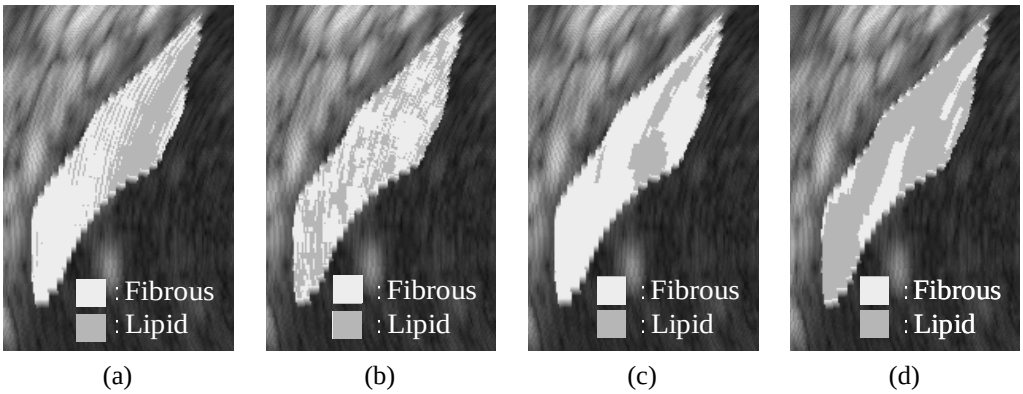


Fig. 16. Tissue characterization results for the lipid tissue. (a) IB method; (b) kNN method; (c) Fourier spectrum analysis method; (d) Proposed method (ASSOM).

[5] B. N. Potkin, A. L. Bartorelli, J. M. Gessert, R. F. Neville, Y. Almagor, W. C. Roberts, M. B. Leon, "Coronary artery imaging with intravascular high-frequency ultrasound," *Circulation*, vol.81, pp.1575-1585, 1990.

[6] J. M. Tobis, J. Mallery, D. Mahon, K. Lehmann, P. Zalesky, J. Griffith, J. Gessert, M. Moriuchi, M. McRae, M. L. Dwyer, "Intravascular ultrasound imaging of human coronary arteries in vivo: Analysis of tissue characterizations with comparison to in vitro histological specimens," *Circulation*, vol.83, pp.913-926, 1991.

[7] S. E. Nissen, J. C. Gurley, C. L. Grines, D. C. Booth, R. McClure, M. Berk, C. Fischer, A. N. DeMaria, "Intravascular ultrasound assessment of lumen size and wall morphology in normal subjects and patients with coronary artery disease," *Circulation*, vol.84, pp.1087-1099, 1991.

[8] D. T. Linker, A. Klevan, Å. Grønningsæther, P. G. Yock, Bj. A. J. Angelsen, "Tissue characterization with intra-arterial ultrasound: Special promise and problems," *Int. J. Cardiac Imaging*, vol.6, pp.255-263, 1991.

[9] M. Sonka, X. Zhang, M. Siebes, M. S. Bissing, S. C. DeJong, S. M. Collins, C. R. McKay, "Segmentation of intravascular ultrasound images: A knowledge-based approach," *IEEE Trans. on Medical Imaging*, vol.14, pp.719-732, 1995.

[10] J. D. Klingensmith, D. G. Vince, B. D. Kuban, R. Shekhar, E. M. Tuzcu, S. E. Nissen, J. F. Cornhill, "Assessment of coronary compensatory enlargement by three-dimensional intravascular ultrasound," *Int. J. Cardiac Imaging*, vol.16, pp.87-98, 2000.

[11] S. J. Nicholls, E. M. Tuzcu, I. Sipahi, P. Schoenhagen, S. E. Nissen, "Intravascular ultrasound in cardiovascular medicine," *Circulation*, vol.114, pp.54-59, 2006.

[12] M. Kawasaki, H. Takatsu, T. Noda, K. Sano, Y. Ito, K. Hayakawa, K. Tsuchiya, M. Arai, K. Nishigaki, G. Takemura, S. Minatoguchi, T. Fujiwara, H. Fujiwara, "In vivo quantitative tissue characterization of human coronary arterial plaques by use of integrated backscatter intravascular ultrasound and comparison with angioscopic findings," *Circulation*, vol.105, pp.2487-2492, 2002.

[13] K. Sano, M. Kawasaki, M. Okubo, H. Yokoyama, Y. Ito, I. Murata, T. Kawai, K. Tsuchiya, K. Nishigaki, G. Takemura, S. Minatoguchi,

X. Zhou, H. Fujita, H. Fujiwara, “In vivo quantitative tissue characterization of angiographically normal coronary lesions and the relation with risk factors: A study using integrated backscatter intravascular ultrasound,” *Circulation J.*, vol.69, pp.543-549, 2005.

[14] M. P. Moore, T. Spencer, D. M. Salter, P. P. Kearney, T. R. D. Shaw, I. R. Starkey, P. J. Fitzgerald, R. Erbel, A. Lange, N. W. McDicken, G. R. Sutherland, K. A. A. Foxa, “Characterisation of coronary atherosclerotic morphology by spectral analysis of radiofrequency signal: in vitro intravascular ultrasound study with histological and radiological validation,” *Heart*, vol.79, pp.459-467, 1998.

[15] A. Nair, B. D. Kuban, E. M. Tuzcu, P. Schoenhagen, S. E. Nissen, D. G. Vince, “Coronary plaque classification with intravascular ultrasound radiofrequency data analysis,” *Circulation*, vol.106, pp.2200-2206, 2002.

[16] R. O. Duda, P. E. Hart, D. G. Stork, *Pattern Classification*, 2nd ed. John Wiley & Sons, 2001.

[17] B. Huang, A. Ahuja, H. L. Huang, T. J. Schmit, R. W. Heymann, “Mean-removed nearest neighbor reordering based lossless compression of 3D hyperspectral sounder data,” *WSEAS Trans. on Circuits and Systems*, vol.3, pp.858-866, 2004.

[18] F. Kovacs, R. Ivancsy, “A novel cluster validity index: Variance of the nearest neighbor distance,” *WSEAS Trans. on Computers*, vol.5, pp.477-483, 2006.

[19] T. M. Cover, P. E. Hart, “Nearest neighbor classification,” *IEEE Trans. on Information Theory*, vol.IT-13, pp.21-27, 1967.

[20] K. Fukunaga, “Bias of nearest neighbor error estimation,” *IEEE Trans. on Pattern Analysis and Machine Intelligence*, vol.9, pp.103-112, 1987.

[21] P. E. Hart, “The condensed nearest neighbor rule,” *IEEE Trans. on Information Theory*, vol.IT-14, pp.515-516, 1968.

[22] G. W. Gates, “The reduced nearest neighbor rule,” *IEEE Trans. on Information Theory*, vol.IT-18, pp.431-433, 1972.

[23] T. Kohonen, “Emergence of invariant feature detectors in the adaptive-subspace self-organizing map,” *Biol. Cybern.*, vol.75, pp.281-291, 1996.

[24] T. Kohonen, “Self-organized formation of topological correct feature maps,” *Biol. Cybern.*, vol.43, pp.59-69, 1982.

[25] T. Kohonen, *Self-Organizing Maps*, Springer-Verlag, Berlin, 1995.

[26] T. Kohonen, S. Kaski, H. Lappalainen, “Self-organized formation of various invariant-feature filters in the adaptive-subspace SOM,” *Neural Computation*, vol.9, pp.1321-1344, 1997.

[27] S. Kaski, J. Kangas, T. Kohonen, “Bibliography of self-organizing map (SOM) papers: 1981-1997,” *Neural Computing Surveys*, vol.1, pp.102-350, 1998.

[28] J. L. Giraudel, V. D. Boishebert, M. Montury, “Application of self-organizing map algorithm combined with structuring index to characterize strawberry variety aroma by SPME/GC/MS,” *WSEAS Trans. on Systems*, vol.3, pp.461-466, 2004.

[29] A. Hyvärinen, P. Hoyer, “Emergence of phase- and shift-invariant features by decomposition of natural images into independent feature subspaces,” *Neural Computation*, vol.12, pp.1705-1720, 2000.

[30] Z. Q. Liu, “Adaptive subspace self-organizing maps and its applications in face recognition,” *Int. J. of Image and Graphics*, vol.2, pp.519-540, 2002.

[31] R.A. Schowengerdt, Remote Sensing. Models and Methods for Image Processing, 2nd ed. Academic Press, New York, 1997.

[32] J. C. Russ, *The Image Processing Handbook*, 5th ed. Academic Press, New York, 2006.